Inorg. Chem. **2007**, *46*, 5398–5403

Tetrairon and Hexairon Hydroxo/Acetato Clusters Stabilized by Multiple Polyoxometalate Scaffolds. Structures, Magnetic Properties, and Chemistry of a Dimer and a Trimer

Bogdan Botar,[†] Paul Kögerler,[‡] and Craig L. Hill*[,†]

Department of Chemistry, Emory University, Atlanta, Georgia 30322, and Ames Laboratory, Iowa State University, Ames, Iowa 50011

Received January 25, 2007

Investigation of the catalytically relevant γ-diiron(III) Keggin complexes in aqueous acetate buffer leads to a dimeric C_{2v}-symmetric polyanion, $[\{Fe(OH)(OAc)\}_4(\gamma\text{-}SiW_{10}O_{36})_2]^{12-}$ (**3**) and a trimeric C_2-symmetric polyanion, $[\{Fe_6(OH)_9(H_2O)_2(OAc)_2\}(\gamma\text{-}SiW_{10}O_{36})_3]^{17-}$ (**4**). Polyanion **3** incorporates a hydroxo/acetato-bridged tetrairon(III) core, while **4** incorporates a trigonal prismatic hydroxo/acetato-bridged hexairon(III) core. The monomeric building unit of **3** and **4**, $\{\gamma\text{-}SiW_{10}Fe_2\}$, adopts the "out-of-pocket" structural motif (with two corner-sharing FeO_6 coordination polyhedra no longer connected to the internal SiO_4 tetrahedron of the Keggin unit) also observed in the $\{\gamma\text{-}SiW_{10}Fe_2\}$-type structures isolated from nonbuffered aqueous solutions. Following hydrolysis, **3** is converted to **4** as confirmed by ^{29}Si NMR. Magnetic measurements establish that in both **3** and **4** all exchange interactions are antiferromagnetic.

Introduction

Interest in polyoxometalate (POM) chemistry derives from potential applications in catalysis, magnetism, and materials science.[1−6] As a consequence of their thermodynamic stability to oxidative degradation, an attribute not shared by organic structures, POMs have been used as efficient and selective catalysts for oxidation reactions of organic substrates using the most desirable and environmentally acceptable oxidants, O_2 and H_2O_2.[6−12] Among these catalytic systems, those containing the divacant silicodecatungstate Keggin anion, γ-SiW_{10}[13,14] and its dimetal substituted (dimetallo) derivatives, γ-$SiW_{10}M_2$ (M = Ti(IV), V(V), Mn(III), and Fe(III))[15−21] occupy a prominent role. All these

* To whom correspondence should be addressed. E-mail: chill@emory.edu.
† Emory University.
‡ Iowa State University.

(1) *Polyoxometalates: from Platonic Solids to Anti-Retroviral Activity*; Pope, M. T., Müller, A., Eds.; Kluwer: Dordrecht, The Netherlands, 1994.
(2) Topical issue on polyoxometalates: Hill, C. L. *Chem. Rev.* **1998**, *98*, 1−389.
(3) *Polyoxometalate Chemistry: From Topology via Self-Assembly to Applications*; Pope, M. T., Müller, A., Eds.; Kluwer: Dordrecht, The Netherlands, 2001.
(4) *Polyoxometalate Chemistry for Nanocomposite Design*; Yamase, T., Pope, M. T., Eds.; Kluwer Academic/Plenum Publishing: New York, 2002.
(5) Pope, M. T. Polyoxo Anions: Synthesis and Structure. In *Comprehensive Coordination Chemistry II: Transition Metal Groups 3−6*; Wedd, A. G., Ed.; Elsevier Science: New York, 2004; Vol. 4, Chapter 4.10, pp 635−678.
(6) Hill, C. L. In *Comprehensive Coordination Chemistry II: From Biology to Nanotechnology*; Wedd, A. G., Ed.; Elsevier: Oxford, 2004; Vol. 4, pp 679−759.
(7) Hill, C. L.; Prosser-McCartha, C. M. *Coord. Chem. Rev.* **1995**, *143*, 407−455.
(8) Neumann, R. *Prog. Inorg. Chem.* **1998**, *47*, 317−370.
(9) Okuhara, T.; Mizuno, N.; Misono, M. *Adv. Catal.* **1996**, *41*, 113−252.
(10) Mizuno, N.; Misono, M. *Chem. Rev.* **1998**, *98*, 199−218.
(11) Moffat, J. B. *Metal-Oxygen Clusters: The Surface and Catalytic Properties of Heteropoly Oxometalates.*; Kluwer Academic/Plenum Publishers: New York, 2001; Vol. 9.
(12) Kozhevnikov, I. V. *Catalysis by Polyoxometalates*; Wiley: Chichester, 2002; Vol. 2.
(13) Kamata, K.; Yonehara, K.; Sumida, Y.; Yamaguchi, K.; Hikichi, S.; Mizuno, N. *Science* **2003**, *300*, 964−966.
(14) Prabhakar, R.; Morokuma, K.; Hill, C. L.; Musaev, D. G. *Inorg. Chem.* **2006**, *45*, 5703−5709.
(15) Goto, Y.; Kamata, K.; Yamaguchi, K.; Uehara, K.; Hikichi, S.; Mizuno, M. *Inorg. Chem.* **2006**, *45*, 2347−2356.
(16) Nakagawa, Y.; Uehara, K.; Mizuno, N. *Inorg. Chem.* **2005**, *44*, 14−16.
(17) Nakagawa, Y.; Uehara, K.; Mizuno, N. *Inorg. Chem.* **2005**, *44*, 9068−9075.
(18) Nakagawa, Y.; Kamata, K.; Kotani, M.; Yamaguchi, K.; Mizuno, N. *Angew. Chem., Int. Ed.* **2005**, *44*, 5136−5141.
(19) Hayashi, T.; Kishida, A.; Mizuno, N. *Chem. Commun.* **2000**, 381−382.
(20) Mizuno, N.; Nozaki, C.; Kiyoto, I.; Misono, M. *J. Am. Chem. Soc.* **1998**, *120*, 9267−9272.
(21) Nishiyama, Y.; Nakagawa, Y.; Mizuno, N. *Angew. Chem., Int. Ed.* **2001**, *40*, 3639−3641.

10.1021/ic070126y CCC: $37.00
Published on Web 05/23/2007

dimetallo derivatives contain two proximal and synergistically interacting centers, a feature also observed in several enzymes including methane monooxygenase (MMO)[22−27] and ribonucleotide reductase (RNR),[28−31] that are of intense current research interest. It is, therefore, not surprising that in addition to structural investigations and catalytic properties, magnetic measurements and computational studies have been carried out in order to garner additional insight into their complex electronic and magnetic structures.[32,33] The report by Mizuno et al. on selective reductant-free aerobic oxidation of alkenes catalyzed by an organic-solvent-soluble POM complex [γ(1,2)-$SiW_{10}\{Fe(OH_2)\}_2O_{38}]^{6-}$ (**1**) has attracted considerable interest.[21] Very recently, we clarified issues and challenges posed by the chemistry and catalysis of **1**.[34] At the same time, in an attempt to move from catalytic systems using decidedly non-green solvents (catalysis by **1** takes place in a chlorocarbon−acetonitrile solution), we demonstrated that the "aqueous" analogue of **1** exists as an unsymmetric trimer, [$\{Fe_2(OH)_3(H_2O)_2\}_3(\gamma$-$SiW_{10}O_{36})_3]^{15-}$ (**2**).[34] In contrast to **1**, where the two vicinal edge-sharing ferric centers reside in the multidentate polytungstate pocket (the "in-pocket" structure), the iron centers in **2** have moved away from the body of the POM, are corner-sharing and are no longer connected to the internal Si heteroatom oxygens (the "out-of pocket" structure). Significantly, we determined that the trimer, **2**, is a precatalyst for the selective oxidation of sulfur compounds using the environmentally optimal solvent, H_2O, and oxidant, O_2.[34] Since **2** could be just one member of an entire family of attractive water-soluble catalysts, we have sought to investigate the complex aqueous chemistry of the γ-$SiFe_2W_{10}$ in the presence of acetate, an extensively used buffer for aqueous reactions and a ligand that readily bridges metal centers. In doing so, we seek to obtain a better understanding of the geometrical and electronic structures and the magnetic interactions between the vicinal iron centers in the catalytic active site. These features, in aggregate, dictate reactivity and consequently catalytic performance. Within this broad context we report here the synthesis, structure, magnetic properties, and aqueous chemistry of two silicotungstate derivatives incorporating hydroxo/acetato tetrairon and hexairon(III) clusters, [$\{Fe(OH)(OAc)\}_4$-(γ-$SiW_{10}O_{36})_2]^{12-}$ (**3**) and [$\{Fe_6(OH)_9(H_2O)_2(OAc)_2\}$($\gamma$-$SiW_{10}O_{36})_3]^{17-}$ (**4**).

Experimental Section

General Methods and Materials. Potassium γ-decatungstosilicate, $K_8[\gamma$-$SiW_{10}O_{36}]\cdot 12H_2O$,[35] was prepared according to literature methods, and its identity and purity were checked by infrared spectroscopy. Elemental analyses were performed by Kanti Labs (Mississauga, Canada) and Atlantic Microlab, Inc. (Norcross, GA). Infrared spectra (2% sample in KBr) were recorded on a Nicolet 510 FTIR spectrometer. Electronic absorption spectra were recorded on a Hewlett-Packard 8452A diode array spectrophotometer. ^{29}Si NMR spectra (referenced to 3.6 M TMS in $CDCl_3$) were acquired at room temperature using a UNITY 600FT NMR instrument. The pulse width was 0.6 μs, and the relaxation delay was 0.8 s. Differential scanning calorimetric and thermogravimetric data were recorded on ISI DSC 550 and TGA 1000 instruments, respectively. Magnetic measurements were performed for temperature ranges from 2.0 to 290 K and magnetic field ranges from 0.1 to 5.0 Tesla on a Quantum Design MPMS-5 SQUID magnetometer. Experimental susceptibility data were corrected for diamagnetic and TIP (temperature-independent paramagnetic) contributions that were derived both from tabulated increments and from previous measurements on similar diamagnetic polyoxotungstates: $\chi_{dia/TIP}(\mathbf{K_4[(CH_3)_2(NH_2)]_8 3}) = -1.65 \times 10^{-3}$ emu mol^{-1}, $\chi_{dia/TIP}(\mathbf{K_9[(CH_3)_2(NH_2)]_8 4}) = -2.21 \times 10^{-3}$ emu mol^{-1}. Field-dependent magnetization (M vs H) measurements at 2.0 K (equipment base temperature, see Figure S1 in Supporting Information) for compound **3** conform to a scaled $B(s = 5/2)$ Brillouin function. These data suggest the presence of 4.7% per formula unit of an uncoupled $s = 5/2$ species such as a mononuclear Fe(III) complex. No impurity is observed from the M vs H plot for compound **4** (Figure S1 in Supporting Information). The scanning range of exchange parameters used in the adaptive fitting procedure covered values from $J/k_B = -50$ to 0 K with a resolution of 0.1 K; nearest-neighbor spin Hamiltonian terms were of the form $\boldsymbol{H}(\mathbf{3}) = -2J_1(\mathbf{S_1\cdot S_2} + \mathbf{S_3\cdot S_4}) - 2J_2(\mathbf{S_1\cdot S_3} + \mathbf{S_2\cdot S_4})$ and $\boldsymbol{H}(\mathbf{4}) = -2J_1(\mathbf{S_1\cdot S_2} + \mathbf{S_4\cdot S_5}) - 2J_2(\mathbf{S_1\cdot S_3} + \mathbf{S_5\cdot S_6}) - 2J_3(\mathbf{S_2\cdot S_3} + \mathbf{S_4\cdot S_6}) - 2J_4(\mathbf{S_1\cdot S_4} + \mathbf{S_2\cdot S_5}) - 2J_5\mathbf{S_3\cdot S_6}$.

Synthesis of $\mathbf{K_4[(CH_3)_2(NH_2)]_8[\{Fe(OH)(OAc)\}_4(\gamma\text{-}SiW_{10}O_{36})_2]\cdot 16H_2O}$ ($\mathbf{K_4[(CH_3)_2(NH_2)]_8 3}$). Solid $K_8[\gamma$-$SiW_{10}O_{36}]\cdot 12H_2O$ (2.00 g, 0.67 mmol) was quickly added to a solution containing $Fe(NO_3)_3\cdot 9H_2O$ (0.55 g, 1.36 mmol) dissolved in 30 mL of CH_3COOH/CH_3COOK buffer (0.5 M, pH 4.7). The resulting slightly turbid red-brown mixture was stirred for 10 min and then treated with $(CH_3)_2NH_2Cl$ (2.0 g, 24.4 mmol). The solution gradually cleared and after 5 min was filtered off. Red-brown columnar crystals separated after 1 week. Yield ca. 1.2 g (60% based on W). Anal. Calcd (found) for $W_{20}Fe_4K_4Si_2O_{100}N_8C_{24}H_{112}$: W, 59.06 (58.9); Fe, 3.59 (3.79); Si, 0.90 (0.93); K, 2.51 (2.51); N, 1.80 (1.86); C, 4.63 (4.40). IR (KBr pellet; 2000−400 cm^{-1}): 1579 (m-s), 1464 (w), 1417 (m-w), 1384 (w), 1026 (m), 998 (w), 948 (s), 874 (s), 792 (vs), 723 (s), 665 (br, s), 542 (m), 483 (m). UV−vis [λ_{max}, nm (ϵ, M^{-1} cm^{-1})] of a (a) 70 mM fresh solution in H_2O: 445 (220), 550 (sh); (b) 70 mM solution in H_2O incubated for 2 h: 445(160). ^{29}Si NMR (100 mM solution in D_2O at pH 6; ppm): −94.3 ($\delta\nu_{1/2} = 30 \pm 1$ Hz), −94.9 ($\delta\nu_{1/2} = 35 \pm 1$ Hz).

(22) Feig, A. L.; Lippard, S. J. *Chem. Rev.* **1994**, *94*, 759−805.
(23) Costas, M.; Chen. K.; Que, L., Jr. *Coord. Chem. Rev.* **2000**, *200−202*, 517−544.
(24) Siegbahn, P. E. M.; Crabtree, R. H. In *Structure and Bonding*; Springer-Verlag GmbH: Berlin, 2000; Vol. 97, pp 125−144.
(25) Solomon, E. I.; Brunold, T. C.; Davis, M. I.; Kemsley, J. N.; Lee, S.-K.; Lehnert, N.; Neese, F.; Skulan, A. J.; Yang, Y. -S.; Zhou, J. *Chem. Rev.* **2000**, *100*, 235−349.
(26) Merkx, M.; Kopp, D. A.; Sazinsky, M. H.; Blazyk, J. L.; Müller, J.; Lippard, S. J. *Angew. Chem., Int. Ed.* **2001**, *40*, 2782−2807.
(27) Baik, M. -H.; Newcomb, M.; Friesner, R. A.; Lippard, S. J. *Chem. Rev.* **2003**, *103*, 2385−2419.
(28) Que, L., Jr.; Dong, Y. *Acc. Chem. Res*. **1996**, *29*, 190−196.
(29) Sintchak, M. D.; Arjara, G.; Kellogg, B. A.; Stubbe, J.; Drennan, C. L. *Nat. Struct. Biol.* **2002**, *9*, 293−300.
(30) Skulan, A. J.; Brunold, T. C.; Baldwin, J.; Saleh, L.; Bollinger, J. M.; Solomon, E. I. *J. Am. Chem. Soc.* **2004**, *126*, 8842−8855.
(31) Eckert, N. A.; Stoian, S.; Smith, J. M.; Bominaar, E. L.; Münck, E.; Holland, P. L. *J. Am. Chem. Soc.* **2005**, *127*, 9344−9345.
(32) Musaev, D. G.; Morokuma, K.; Geletii, Y. V.; Hill, C. L. *Inorg. Chem.* **2004**, *43*, 7702−7708.
(33) Quiñonero, D.; Wang, Y.; Morokuma, K.; Khavrutskii, L. A.; Botar, B.; Geletii, Y. V.; Hill, C. L.; Musaev, D. G. *J. Phys. Chem. B* **2006**, *110*, 170−173.
(34) Botar, B.; Geletii, Y. V.; Kögerler, P.; Musaev, D. G.; Morokuma, K.; Weinstock, I. A.; Hill, C. L *J. Am. Chem. Soc.* **2006**, *128*, 11268−11277.
(35) Tézé, A.; Hervé, G. In *Inorganic Syntheses*; Ginsberg, A. P., Ed.; John Wiley and Sons: New York, 1990; Vol. 27, pp 85−96.

Synthesis of $K_9[(CH_3)_2(NH_2)]_8[\{Fe_6(OH)_9(H_2O)_2(OAc)_2\}(\gamma\text{-}SiW_{10}O_{36})_3]\cdot 39H_2O$ ($K_9[(CH_3)_2(NH_2)]_8$4). Complex **4** results from decomposition of a highly concentrated (60−100 mM) solution of **3** in water. Authentic **4** is prepared as follows. A 100 mM solution of **3** (3 g of **3** in 5 mL) was kept for 2−3 days in a closed vial. At this stage, a corresponding deuterated solution displays a two-line ^{29}Si NMR spectrum with an intensity ratio of 2:1. Next, the solution was transferred to a beaker and allowed to evaporate in open air at room temperature. Light-green parallelepiped crystals formed after 1−2 days. Yield 2.4 g (80% based on $K_4[(CH_3)_2(NH_2)]_8$**3**). Anal. Calcd (found) for $W_{30}Fe_6K_9Si_3O_{162}N_8C_{20}H_{162}$: W, 58.72 (59.2); Fe, 3.57 (3.46); Si, 0.90 (0.96); K, 3.74 (3.58); N, 1.19 (1.30); C, 2.56 (2.69). IR (KBr pellet; 2000−400 cm^{-1}): 1622 (m-w), 1547 (m-w), 1465 (m-w), 1414 (w), 1024 (m), 998 (m-w), 949 (s), 876 (s), 793 (vs), 725 (s), 533 (m), 484 (m).

X-ray Crystallography. Crystals of $K_4[(CH_3)_2(NH_2)]_8$**3** and $K_9[(CH_3)_2(NH_2)]_8$**4** were taken directly from the mother liquor and immediately cooled to 173(2) K on a Bruker D8 SMART APEX CCD sealed-tube diffractometer with graphite-monochromated (three-circle goniometer with 1 K CCD detector, Mo Kα (0.71073 Å) radiation). Structure solution and refinement, graphic, and generation of publication materials were performed using SHELX-TL, V 6.12 software.[36] Crystal Data for $K_4[(CH_3)_2(NH_2)]_8$**3**: $W_{20}Fe_4K_4Si_2O_{100}N_8C_{24}H_{112}$, $M = 6226.20$, tetragonal, space group $I4/m$, $a = 37.430(2)$ Å, $c = 19.682(1)$ Å, $V = 27575(3)$ Å^3, $Z = 8$, $\rho = 3.00$ g/cm^3, $\mu = 17.248$ mm^{-1}, F (000) = 22 400, crystal size = 0.14 × 0.11 × 0.10 mm^3. A total of 218 748 reflections (1.54° < Θ < 30.08°) were collected of which 20 749 reflections were unique (R(int) = 0.1191). $R = 0.0620$ for 13 798 reflections with $I > 2\sigma(I)$, $R = 0.0936$ for all reflections; max/min residual electron density 6.39 (0.82 Å from W10) and −2.94 e Å^{-3}. The maximum shift/error value and GOF were 0.001 and 1.03, respectively. **Crystal Data for $K_9[(CH_3)_2(NH_2)]_8$4**: $W_{30}Fe_6K_9Si_3O_{162}N_8C_{20}H_{162}$, $M = 9393.34$, trigonal, space group $P3_121$, $a = 20.3314(9)$ Å, $c = 33.390(3)$ Å, $V = 11953(1)$ Å^3, $Z = 3$, $\rho = 3.915$ g/cm^3, $\mu = 22.464$ mm^{-1}, F (000) = 12 666, crystal size = 0.15 × 0.10 × 0.04 mm^3. A total of 107 393 reflections (1.68° < Θ < 27.10°) were collected of which 17 405 reflections were unique (R(int) = 0.0700). $R = 0.0557$ for 16924 reflections with $I > 2\sigma(I)$, $R = 0.0575$ for all reflections; max/min residual electron density 5.61 (0.85 Å from W11) and −2.59 e Å^{-3}. The maximum shift/error value and GOF were 0.001 and 1.29, respectively. The Flack parameter value of 0.037(2) indicates the correct absolute configuration.

Results and Discussion

Structure and Chemistry of Acetate-Bridged γ-Diiron Keggin POMs. The reaction of $[\gamma\text{-}SiW_{10}O_{36}]^{8-}$ with 2 equiv of Fe(III) in 0.5 M CH_3COOH/CH_3COOK aqueous buffer solution (pH 4.7) at room temperature followed by addition of a hydrogen-bonding cation leads to the formation of a new dimeric γ-diiron(III) polytungstosilicate, **3** (Figure 1). The structure of **3** can be viewed as a C_{2v}-symmetric arrangement of two $\{\gamma\text{-}SiW_{10}\}$ units connected by a hydroxo/acetato-bridged tetrairon(III) core, $[\{Fe(OH)(OAc)\}_4]^{4+}$. The monomeric unit in **3**, $\{\gamma\text{-}SiW_{10}Fe_2\}$, adopts the same "out-of-pocket" structural motif (the iron centers are corner-sharing and no longer ligated to the internal oxygen atoms of the central Si heteroatom) observed in the trimer, **2**, which is obtained following a similar synthetic protocol (identical Fe(III)/SiW_{10} reactant ratio, same type of countercations, and similar pH), but in the absence of any buffer.[34] The iron centers in **3** form a planar arrangement and are connected with each other by hydroxo groups (bond valence sum (BVS) values for the monoprotonated oxygen atoms range between 1.1 and 1.4) and bidentate acetate ligands. The oxidation state (3+) of the Fe centers in **3** has been unambiguously confirmed by (a) the exclusive use of a ferric salt ($Fe(NO_3)_3\cdot 9H_2O$) under aerobic conditions as a starting material; (b) BVS calculations which give values of 3.0−3.1 for the Fe centers; and (c) magnetic measurements (discussed below) which are fully consistent with Fe(III) centers and not Fe(II). The presence of bidentate acetate ligands binding adjacent d-metal cations is reminiscent of the dichromium (III) tungstosilicate derivative, $[\gamma(1,2)\text{-}SiW_{10}O_{36}(OH)\{Cr(H_2O)(OAc)\}_2]^{5-}$, the only known non-iron example of an "out-of-pocket" γ-Keggin derivative.[37] In contrast to the dichromium(III) complex, in **3** the bidentate acetate ligands bind to vicinal iron centers belonging to different polytungstate monomer units. There are only a few other examples of polytungstates containing acetate ligands. These include a multiiron(III)-substituted tungstophosphate, $[H_4P_2W_{12}Fe_9O_{56}(OAc)_7]^{6-}$, a dirhodium(III) derivative, $[PW_{11}O_{39}\{Rh_2(OAc)_2\}]^{5-}$, and three lanthanide-containing complexes: $[\{\alpha_2\text{-}P_2W_{17}O_{61}La(H_2O)_2(OAc)\}_2]^{16-}$ and $[\{SiW_{11}O_{39}Ln(H_2O)(OAc)\}_2]^{12-}$ (Ln = Gd(III), Yb(III)).[38−41] In addition to

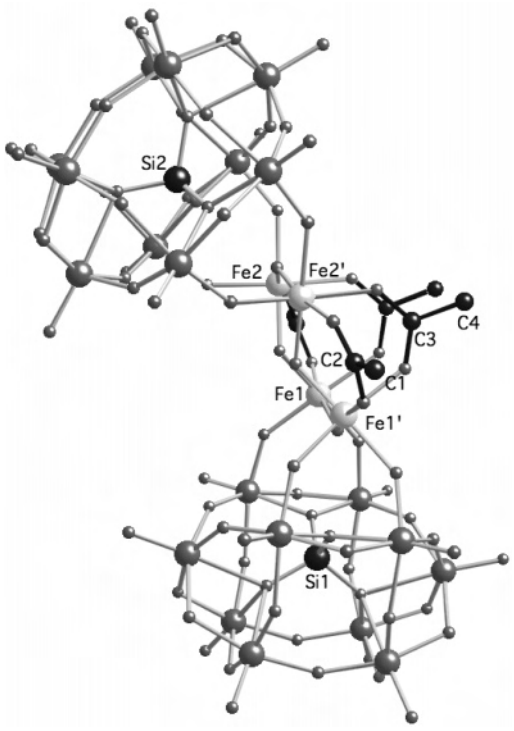

Figure 1. Structure of polyanion **3** in ball-and-stick representation (view approximately perpendicular to the anion's C_2 axis): (W: large dark gray spheres; Fe: large light gray spheres; Si: large black spheres; O: small gray spheres; C: small black spheres).

(36) *SHELXTL 6.12*; Bruker AXS, Inc.: Madison WI, 2002.

(37) Wassermann, K.; Lunk, H. -J.; Palm, R.; Fuchs, J.; Steinfeldt, N.; Stösser, R.; Pope, M. T. *Inorg. Chem.* **1996**, *35*, 3273−3279.

(38) Godin, B.; Chen, Y. -G.; Vaissermann, J.; Ruhlmann, L.; Verdaguer, M.; Gouzerh, P. *Angew. Chem., Int. Ed.* **2005**, *44*, 3072−3075.

(39) Wei, X.; Dickman, M. H.; Pope, M. T. *Inorg. Chem.* **1997**, *36*, 130−131.

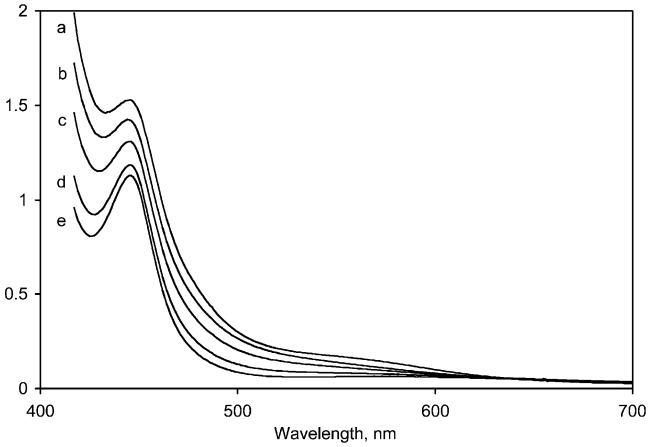

Figure 2. Time profile of the electronic absorption spectra of a 70 mM aqueous solution of $\mathbf{K_4[(CH_3)_2(NH_2)]_8}$**3**: (a) fresh solution and after (b) 5 min, (c) 10 min, (d) 1 h, and (e) 2 h. Spectrum (e) remains virtually unchanged indefinitely.

noteworthy structural features, the dimer, **3**, provides confirmatory evidence to our previous study, which strongly argues in favor of two distinct $\{\gamma\text{-SiW}_{10}\text{Fe}_2\}$ isomers, the "in-pocket" form present in organic solvents and the "out-of-pocket" form present in aqueous solution.[34] This trend can seemingly be expanded to include other dimetallo tungstosilicate derivatives since all "in-pocket" $\{\gamma\text{-SiW}_{10}\text{M}_2\}$ structures (M = Ti(IV), V(V), and Mn(III)) known so far have been isolated from organic solvents.[15,16,42] Interestingly, however, the $[\gamma(1,2)\text{-SiW}_{10}\text{O}_{36}(\text{OH})\{\text{Cr}(\text{H}_2\text{O})(\text{OAc})\}_2]^{5-}$ complex having the "out-of-pocket" dichromium(III) structural motif has been isolated from both H_2O and CH_3CN.[37] Importantly, the structure of **3** also validates our previous computational studies which predicted that the use of ligands with greater binding constants for Fe(III) centers than the $\gamma\text{-SiW}_{10}$ ligand, such as acetate, would result in the cleavage of the Fe−O(Si) bonds and subsequent displacement of the diiron unit out of the polytungstate pocket.[34]

The solution chemistry of **3** was studied using UV−vis and ^{29}Si NMR spectroscopy. The acetate dimer, **3**, is unstable in water, as shown by the time-dependent UV−vis spectra of a 70 mM solution. The spectrum of a fresh sample (taken within seconds after dissolving **3** in water) shows Fe(III)-centered d−d transition bands with a broad shoulder at ca. 550 nm and a peak at 445 nm (Figure 2). Within a few minutes, the profile of the spectrum changes with a gradual disappearance of the shoulder at 550 nm and a decrease in intensity of the peak at 445 nm.

These spectral changes are associated with a change in the solution color from brown to light green. After 2 h, the hydrolytic decomposition seems to be complete and the spectrum does not undergo any further changes. The paramagnetism of the Fe(III) centers has two principal consequences on the ratio of signal-to-noise in the ^{29}Si NMR spectrum of **3**: it shortens the T_1 and T_2 values, which leads

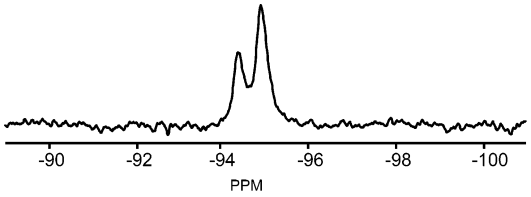

Figure 3. ^{29}Si NMR spectrum of a 100 mM solution of $\mathbf{K_4[(CH_3)_2(NH_2)]_8}$**3** after ca. 4 h. This spectrum remains virtually unchanged after 20 days.

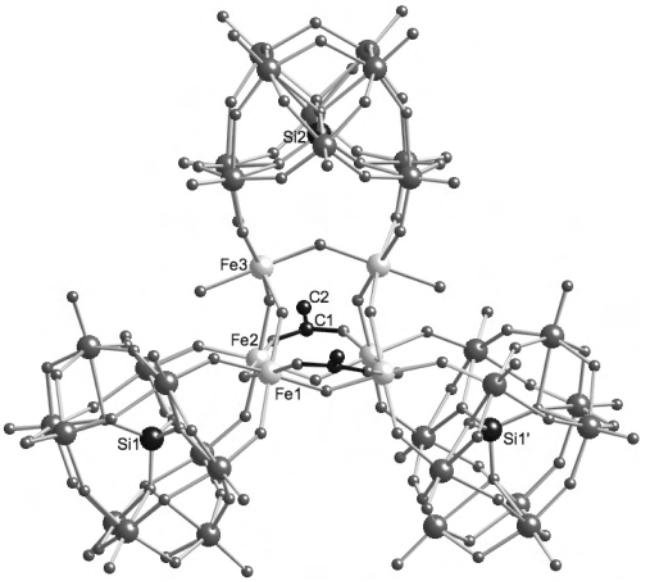

Figure 4. Structure of polyanion **4** in ball-and-stick representation (view perpendicular to the C_2 axis of the polyanion): (W: large dark gray spheres; Fe: large light gray spheres; Si: large black spheres; O: small gray spheres; C: small black spheres).

to much broader lines (decreasing the signal-to-noise), but simultaneously the shorter relaxation time facilitates use of a shorter relaxation delays, etc. (increasing the signal-to-noise ratio due to faster pulsing). Regardless, however, it is clear from the relative rates of **3** converting to **4** and the NMR acquisition time that ^{29}Si NMR cannot provide information on the structure of **3** in solution. The ^{29}Si NMR spectrum shows two resonances with a 2:1 ratio, at −94.3 and −94.9 ppm, respectively (Figure 3). The spectrum of the same solution kept for 20 days is practically identical to that shown in Figure 3. Room-temperature evaporation of the ^{29}Si NMR solution after 1−2 days afforded greenish crystals in a nearly quantitative yield (80% based on **3**).

A single-crystal X-ray structural investigation reveals a trimeric hexairon(III) polyanion, formulated as $[\{\text{Fe}_6(\text{OH})_9(\text{H}_2\text{O})_2(\text{OAc})_2\}(\gamma\text{-SiW}_{10}\text{O}_{36})_3]^{17-}$ (**4**) (Figure 4). The anion structure can be viewed as a trigonal arrangement of three $\{\gamma\text{-SiW}_{10}\}$ units connected by an electrophilic hydroxo/acetato-bridged hexairon(III) central core, $[\text{Fe}_6(\text{OH})_9(\text{H}_2\text{O})_2(\text{OAc})_2]^{7+}$, with overall C_2 symmetry. Significantly, polyanion **4** is quasi-isostructural with the trimer **2**. The only major structural difference between the two polyanions (**2** and **4**) is the incorporation of two bidentate ligands in **4**, which bind two vicinal iron(III) centers from the two symmetry-equivalent, divacant $\{\gamma\text{-SiW}_{10}\}$ units. Like **2**, the acetate-trimer **4**, is also enantiopure (chiral $P3_121$ space

(40) Kortz, U. *J. Cluster Sci.* **2003**, *14*, 205−214.
(41) Mialane, P.; Dolbecq, A.; Riviére, E.; Marrot, J.; Sécheresse, F. *Eur. J. Inorg. Chem.* **2004**, 33−36.
(42) Zhang, X. Y.; O'Connor, C. J.; Jameson, G. B.; Pope, M. T. *Inorg. Chem.* **1996**, *35*, 30−34.

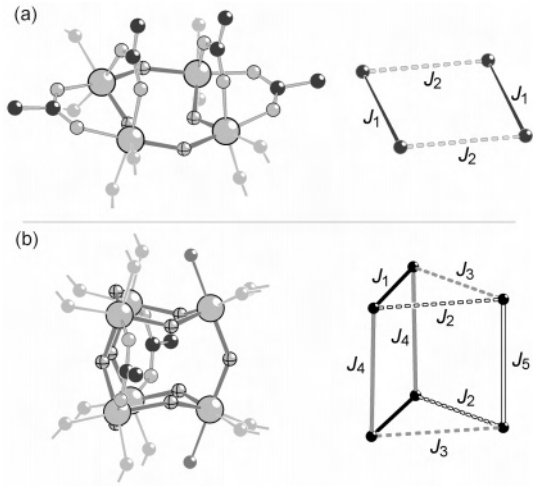

Figure 5. (a) Left: Ball-and-stick representation of the central $\{Fe^{III}_4\}$ core of **3** (Fe: large, bright gray spheres; μ-oxo positions of hydroxo groups: small crossed gray spheres; oxo positions: small gray spheres; C: black spheres; H not shown for clarity). Fe−O−Fe bonds between the inner $\{Fe^{III}_4\}$ fragment are highlighted in dark gray. Right: Corresponding exchange coupling scheme for **3** with the two assigned magnetic superexchange constants reflecting the C_{2v} symmetry of the central $[\{Fe(OH)(OAc)\}_4]^{4+}$ fragment. (b) Left: Structure of the central $\{Fe^{III}_6\}$ core in **4** (oxo positions of terminal H_2O ligands: dark gray; see (a) for other color codes). Right: Exchange coupling scheme for **4** employing five exchange constants, reflecting the C_2 symmetry of the central $[Fe_6(OH)_9(H_2O)_2(OAc)_2]^{7+}$ fragment.

group) as a result of the slight rotation of the two symmetry-equivalent $\{\gamma\text{-}SiW_{10}\}$ units around the C_2 axis of the polyanion. This deviation is about 4.3°, as indicated by the dihedral angle of the least-square planes defined by [O57, Si2, O49, and Fe3] and [Fe3, W15, Si1, and W6] (see Figure S2 in Supporting Information). The observed chirality very likely results from crystal packing forces. The structural similarity of **2** and **4** is also illustrated by their IR spectra, which are virtually identical in the 500−1000 cm^{-1} region (see Figure S3 in Supporting Information). The same arguments used for **3** unambiguously establish the oxidation state as 3+ for the Fe centers in **4**. All μ-oxygen atoms connecting the Fe(III) centers in the hexairon core are monoprotonated with BVS values of 1.1−1.2. The terminal water molecules on the Fe centers are also clearly identified by their corresponding small BVS values of 0.4. The presence of two structurally inequivalent Si atoms (Si1 and Si2 in Figure 4) observed in the solid-state structure of **4** is in agreement with the two-line ^{29}Si NMR spectrum (relative intensity ratio of 2:1) shown by the solution from which crystals of **4** are obtained (Figure 3). This strongly suggests that the acetate trimer, **4**, is indeed the hydrolysis product of **3**. Interestingly, the ^{29}Si NMR corresponding to the acetate-free trimer, **2**, also shows the expected two-line spectrum with a relative intensity ratio of 2:1 but with the more intense peak shifted upfield relative to the other peak.[34] The separation between the two peaks is also different, 1.5 ppm for **2** and 0.6 ppm for **4**. The most likely explanation for the different NMR spectra is that incorporation of the two acetate ligands in **4** affects the interactions between the ferric centers (also addressed below by magnetic studies). A stronger paramagnetic effect is observed in the spectrum of **4** relative to that of **2**, as indicated by the slightly broader NMR lines (30−35 Hz for **4** vs 20−25 Hz for **2**). The ^{29}Si NMR establishes that the trimer structure is stabilized in aqueous solution by the presence of acetate. Specifically, whereas **2** decomposes readily and irreversibly in water, **4** does not. Significantly, this fact provides additional evidence that the catalytic oxidation activity in $\{\gamma\text{-}SiW_{10}Fe_2\}$-derived systems does not involve the trimer itself but a hydrolytic product of the trimer.[34]

Magnetic Properties of 3 and 4. The magnetic properties of **3** and **4** are characterized by antiferromagnetic coupling between the four planar Fe(III) centers of the $\{Fe(OH)(OAc)\}_4$ core and the six Fe(III) centers of the trigonal prismatic $\{Fe_6(OH)_9(H_2O)_2(OAc)_2\}$ core, respectively (Figure 5). As in both **3** and **4**, the Fe centers occupy near-ideal octahedral coordination environments (Fe−O bond lengths of 1.97(1)−2.07(1) Å, O−Fe−O bond angles of 85.8(5)−93.6(5)°), they represent near-ideal spin-5/2 centers in their $^6A_1$ ground states with no significant spin−orbit coupling. The intramolecular exchange is mediated by the single μ-hydroxo group and bridging acetate ligands, which connect the nearest-neighbor iron positions. On the basis of the C_{2v}

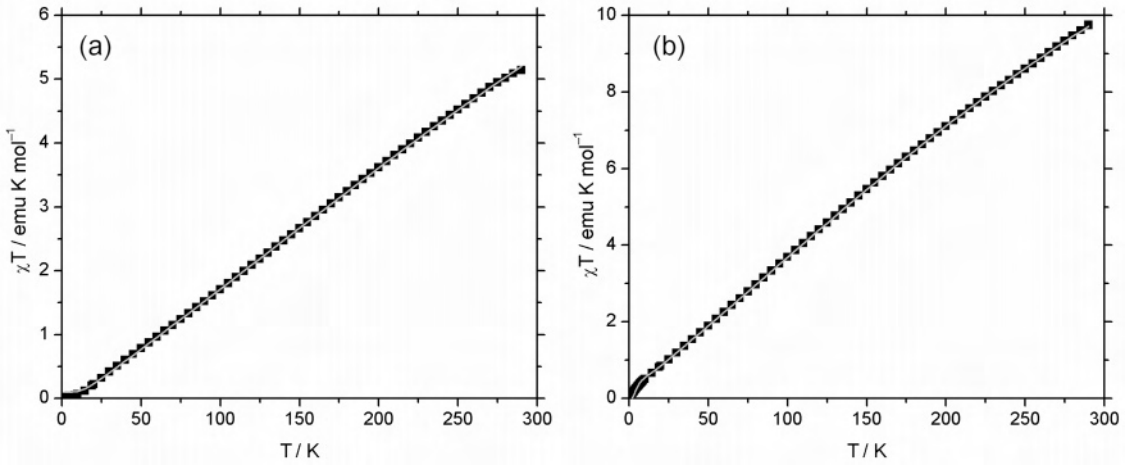

Figure 6. Temperature dependence of χT for compounds $\mathbf{K_4[(CH_3)_2(NH_2)]_8 3}$ (a) and $\mathbf{K_9[(CH_3)_2(NH_2)]_8 4}$ (b) at 0.1 Tesla for the temperature range 2−290 K. Experimental data (corrected for diamagnetic/TIP contributions and, in the case of $\mathbf{K_4[(CH_3)_2(NH_2)]_8 3}$, for paramagnetic components, see Experimental Section): black squares; best fits to the corresponding isotropic Heisenberg models: gray lines.

symmetry of the $\{Fe(OH)(OAc)\}_4$ core of **3**, an isotropic Heisenberg model was adopted that employs two exchange constants, J_1 and J_2, where the two exchange interactions involving one μ-hydroxo and two μ-acetate groups are assigned to J_1 and the two interactions involving only one μ-hydroxo group to J_2 (Figure 5a). For **4**, correspondingly, five exchange constants (J_1-J_5) were used to accommodate the C_2 symmetry of the nine nearest-neighbor interactions in the central $\{Fe_6(OH)_9(H_2O)_2(OAc)_2\}$ fragment. Here, four different Fe−OH−Fe geometries were correlated with J_1, J_2, J_3, and J_5, whereas the Fe(III) pairs coupled by one μ-hydroxo group and one μ-acetate group were assigned to J_4 (Figure 5b). A full computational simulation of the parameter space (i.e., the individual J_n energies and a common, isotropic g factor) yielded a best fit to the low-field susceptibility data for **3** and **4** (Figure 6). Interestingly, the best fit for **3** results in stark differences for $J_1/k_B = -41.2$ K and $J_2/k_B = -4.5$ K, underlining the amplification of antiferromagnetic coupling by the two acetate groups per Fe−Fe contact. For **4**, a best fit is achieved for a set of exchange energies $J_1/k_B = -32.0$ K, $J_2/k_B = -24.0$ K, $J_3/k_B = -18.0$ K, $J_4/k_B = -16.0$ K, and $J_5/k_B = -20.7$ K (all $\pm$ 0.5 K). In both cases, an isotropic splitting factor, $g_{iso} = 1.99$, and a resulting singlet ground state are found. The J values of **4** are similar to the corresponding set of exchange energies observed for the acetate-free trimer, **2**, with its $\{Fe_6(OH)_9(H_2O)_6\}$ core and its identical superexchange connectivity. However, a quantitative comparison is complicated by the fact that due to the relatively large number of exchange parameters, several sets of J_{1-5} all reproduce virtually the same magnetic level spectrum and thus the same thermodynamic parameters (in this case, the temperature dependence of the susceptibility). Corresponding manifolds of local minima then limit the principal accuracy of the finite-resolution fitting procedure. Additional experiments (e.g., low-temperature magnetization measurements, inelastic neutron scattering) are thus necessary to confirm the magnetic level spectrum derived from the particular set of J_{1-5}.

Conclusions

Attempts to expand the γ-diiron(III) Keggin family of catalysts and elucidate their related complex chemistry led to two new multiiron(III) derivatives which incorporate a tetrairon(III) core in **3** and a hexairon(III) core in **4**. As indicated by ^{29}Si NMR, hydrolytic decomposition of **3** leads to the formation of **4** in nearly quantitative yield. The use of aqueous acetate buffer solutions for the preparation of **3** and **4** leads to the incorporation of acetate groups in the POM framework. The acetate groups bind to vicinal ferric centers, thus defining a simple and efficient route for functionalizing the γ-diiron(III) Keggin structures with implications for their magnetic properties and reactivity. The "out-of-pocket" $\{\gamma$-$SiW_{10}Fe_2\}$ structural motif previously observed in the trimer **2**, isolated from nonbuffered aqueous solutions, is confirmed by the X-ray structures of **3** and **4**. These findings corroborate the conclusions of our previous studies and strongly argue in favor of two structural motifs for γ-diiron Keggin derivatives: an "in-pocket" structure observed in organic solvents and an "out-of-pocket" structure observed in both buffered and unbuffered aqueous solutions. In future studies, the findings of this work will be used to evaluate the impact of local metal stereochemistry ("in-pocket" vs "out-of-pocket") on magnetic, catalytic, and other properties of POMs with adjacent metal centers. The examples of the acetate trimer, **4**, and the quasi-isostructural acetate-free trimer, **2**, provide an opportunity to systematically study the influence of functional groups on intramolecular spin exchange between paramagnetic centers in multimetal POMs.

Acknowledgment. We thank the Department of Energy (Grant No. DE-FG02-03ER15461) for support of this research. Ames Laboratory is operated for the U.S. Department of Energy by Iowa State University under Contract No. W-7405-Eng-82.

Supporting Information Available: Additional experimental details, magnetization curves (Figure S1), ball-and-stick structure of **4** (Figure S2), IR spectra of **2** and **4** (Figure S3), and crystallographic files for $\mathbf{K_4[(CH_3)_2(NH_2)]_8}$**3** and $\mathbf{K_9[(CH_3)_2(NH_2)]_8}$**4** in CIF format. This material is available free of charge via the Internet at http://pubs.acs.org.

IC070126Y